ADVANCED OPTICAL MATERIALS
www.advopticalmat.de

# Pyrene-Based Polyimide Covalent Organic Framework with Temperature-Dependent Fluorescence

*Amin Zadehnazari, Ahmadreza Khosropour, Ataf Ali Altaf, Saeed Amirjalayer, and Alireza Abbaspourrad**

**The synthesis of a fluorescent covalent organic framework (COF) using perylene and pyrene building blocks (PEPy-COF), via a one-pot condensation reaction is reported. PEPy-COF is crystallized into 2D nanosheets with a cubic and prismatic crystalline morphology and demonstrates structural stability at temperatures up to 500 °C. The structural morphology is confirmed using X-ray diffraction and atomic-level simulations. These 2D porous polymer sheets form a tetragonal framework that is found to have a high specific surface area of 772 $m^2$ $g^{-1}$. Based on the definition of porous materials, the network is mesoporous with an observed pore size of 3.03 nm, which is in good agreement with the material's calculated pore size. The experimentally obtained HOMO-LUMO band gap is 2.62 eV, confirming the semiconducting nature of PEPy-COF. PEPy-COF emits a shiny blue luminescence under UV and visible light. This luminescence intensity is temperature-dependent in solvents with different polarities and dielectric constants demonstrating that the PEPy-COF has potential use in a wide range of temperature-sensing devices. The fluorescence intensity ratio is similar for different temperatures under ultra-sound conditions and varying solvents.**

## 1. Introduction

The past decade has witnessed the fabrication of various types of covalent organic frameworks (COF) many of which are formed through the condensation polymerization reactions of polyaromatic starting materials.[1] These polymeric materials have been used across multiple fields and applications.[2,3] Recently, COFs containing $\pi$-conjugated structural units exhibiting fluorescence properties have gained attention due in large part to their high chemical and physical stability and tunability.[4]

The properties of COFs are determined by their building blocks or fluorophore units and their geometric arrangements. Fluorescent COFs usually have high electron rich $\pi$-conjugated units such as triphenylene,[5] tetraphenylene,[6,7] pyrene,[8] porphyrin,[9] phenyl hydrazone,[10] carbazole,[11] and phthalocyanine.[12] The design and fabrication of conjugated networks is one method to enhance and tune the fluorescent emissions of COFs. Combining fluorescence with temperature sensing in the design of new COFs has gained significant attention.[13] Usually, optical materials which are used to determine temperature variations, are based on edge absorption shift,[14] refractive index change,[15] or maximum emission wavelength intensity under temperature changes.[16] Examples of the first category include Fabry–Pérot interferometers (resonators),[17] extrinsic Fabry–Pérot interferences,[18] fiber Sagnac interferometers,[19] Mach–Zehnder interferometers,[20] optical fiber interferometric sensors,[21] fiber grating sensors,[22] long-period fiber gratings,[23] surface plasmon resonance sensors,[24] silicon-on-insulator sensors,[25] and thermochromic materials.[26] Temperature-dependent fluorescent materials are also categorized into two types: transition-metal inorganic chromophores, such as Europium,[27] and organic molecules such as organic polymers[28] and COFs.[29] Of these two, very few papers have focused on temperature-dependent fluorescent COFs.[23]

Most of the reported COFs that have shown fluorescence contain boronic ester and imine bonds.[30,31] These COFs are unstable under moist, acidic, and basic conditions, making them unsuitable as fluorescent sensors.[32] Ideally, COFs used as sensors should have high physical, chemical, and thermal stability, large surface area, and low density.[33] To the best of our knowledge, the fluorescent polyimide COFs that have been synthesized so far, have only been used for the detection of chemicals such as trinitrophenol explosives, amines, the detection of $Fe^{3+}$, and the electrochemical detecting of $Pb^{2+}$.[34–37]

We report here a new temperature-dependent fluorescent polyimide COF using perylene and pyrene building blocks (PEPy-COF) to form a tetragonal mesoporous framework with cubic

A. Zadehnazari, A. Khosropour, A. A. Altaf, A. Abbaspourrad
Department of Food Science
College of Agricultural and Life Sciences
Cornell University
Stocking Hall
Ithaca, NY 14853, USA
E-mail: alireza@cornell.edu
S. Amirjalayer
Westfälische Wilhelms-Universität Münster
Institute for Solid State Theory
Center for Nanotechnology and Center for Multiscale Theory and Computation
Wilhelm-Klemm-Straße 10, 48149 Münster, Germany

The ORCID identification number(s) for the author(s) of this article can be found under https://doi.org/10.1002/adom.202300412

**DOI: 10.1002/adom.202300412**

 

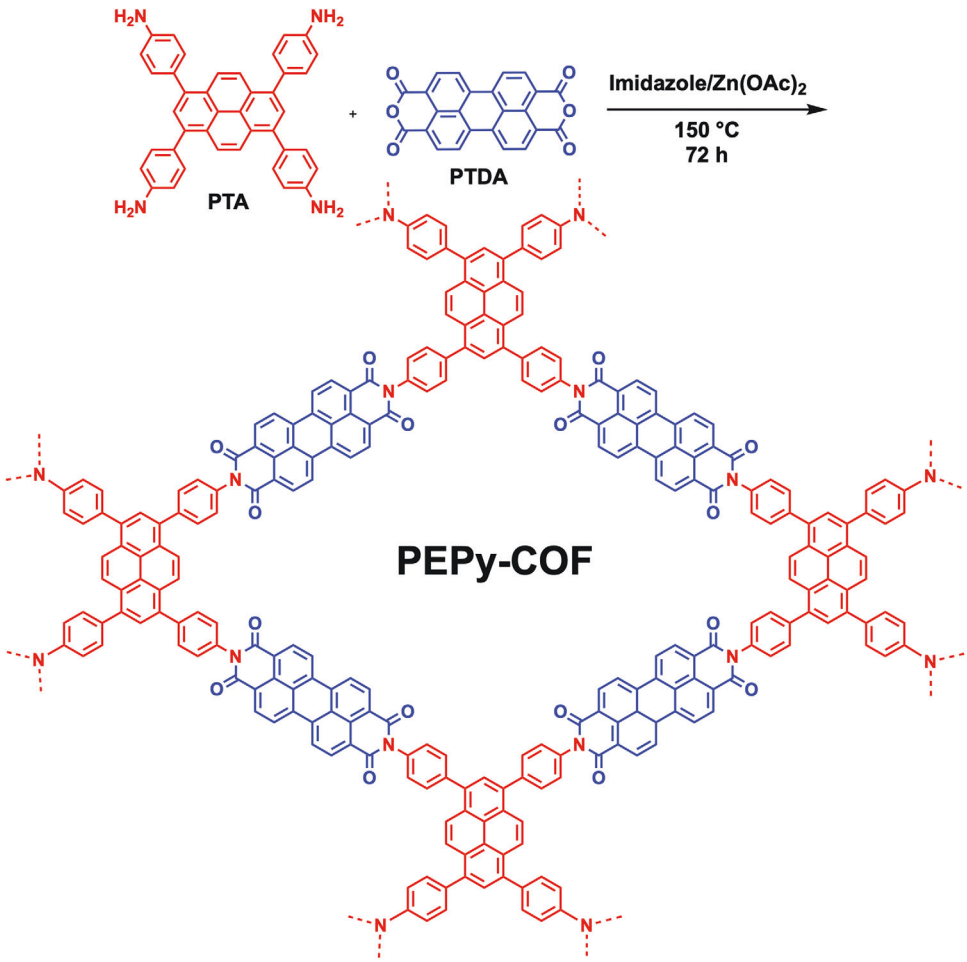


**Scheme 1.** Synthesis of PEPy-COF via a condensation reaction between 4,4′,4″,4‴-(pyrene-1,3,6,8-tetrayl)tetraaniline (PTA) and perylene tetracarboxylic acid dianhydride (PTDA) in imidazole with zinc (II) acetate catalyst.

prismatic morphology (**Scheme 1**). This is the first reported polyimide COF with a temperature-sensitive blue fluorescence emission which is robust to changing solvents and ultrasound treatment.

## 2. Results and Discussion

### 2.1. PEPy-COF Synthesis and Characterization

The PEPy-COF was designed such that the pyrene monomers with $D_{4h}$ symmetry were in the corners geometrically, and the $D_{2h}$ symmetric perylene units were located at the edges of the mesoporous tetragons. PEPy-COF was prepared by the polymerization reaction of perylene tetracarboxylic acid dianhydride (PTDA) and 4,4′,4″,4‴-(pyrene-1,3,6,8-tetrayl)tetraaniline (PTA) in imidazole using zinc acetate [$Zn(OAc)_2$] as a catalyst and was isolated as a brick red powder in 85.4% yield.

The FTIR spectra of our PEPy-COF confirmed the formation of the imide ring (**Figure 1**a). The absorption bands at 1696 and 1660 $cm^{-1}$ were attributed to the asymmetric and symmetric stretches of the carbonyl groups in the six-membered ring. The band at 1372 $cm^{-1}$ was attributed to the imide C–N stretch while the band at 725 $cm^{-1}$ was assigned to C–N bending. The FTIR spectrum of PTDA exhibits the carbonyl stretching frequency at 1758 $cm^{-1}$ which shifts to lower energies in the PEPy-COF spectrum. Further, the peak related to the amine group at 3335 $cm^{-1}$ in PTA, was not present in the PEPy-COF spectrum. Further confirmation of the structure of the reaction product was done using solid-state $^{13}C$ cross-polarization magic-angle spinning nuclear magnetic resonance (CP-MAS ssNMR) spectroscopy. In the ssNMR spectrum of PEPy-COF, the imide carbonyl carbon appeared, as expected, at 160.6 ppm with overlapping peaks for the aromatic carbons appearing between ≈110 and 150 ppm (Figure 1b).[38]

X-ray diffraction (XRD) patterns showed the main diffraction peak at 100 (2.83°), as well as peaks at $10\bar{1}$ (5.07°), 002 (5.77°), $2\bar{2}2$ (7.70°), and 610 (23.17°) (**Figure 2**a). To increase crystallinity, PEPy-COF was treated with supercritical $CO_2$ for 6 h.[39]

To resolve the structure of PEPy-COF, we performed atomistic simulations screening the configurational phase space. We focused on identifying the energetically most preferred packing of the 2D-COFs to determine the energy differences between eclipsed and staggered arrangements. To predict the structure independently from the experimental data, we parametrized

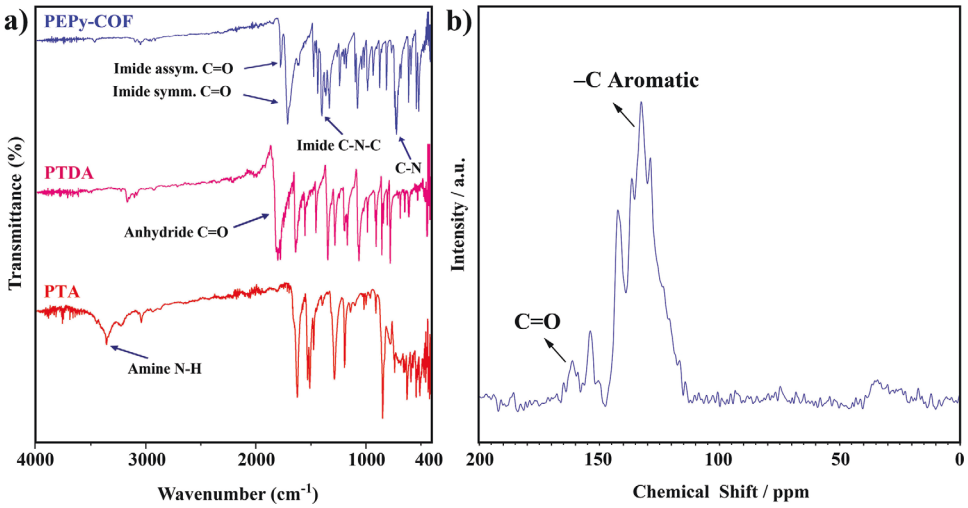


**Figure 1.** a) FT-IR spectra of PEPy-COF (blue), PTDA (pink), and PTA (red), presenting the imide stretching vibrational signals indicating imide heterocycle formation. b) CP-MAS ssNMR of PEPy-COF.

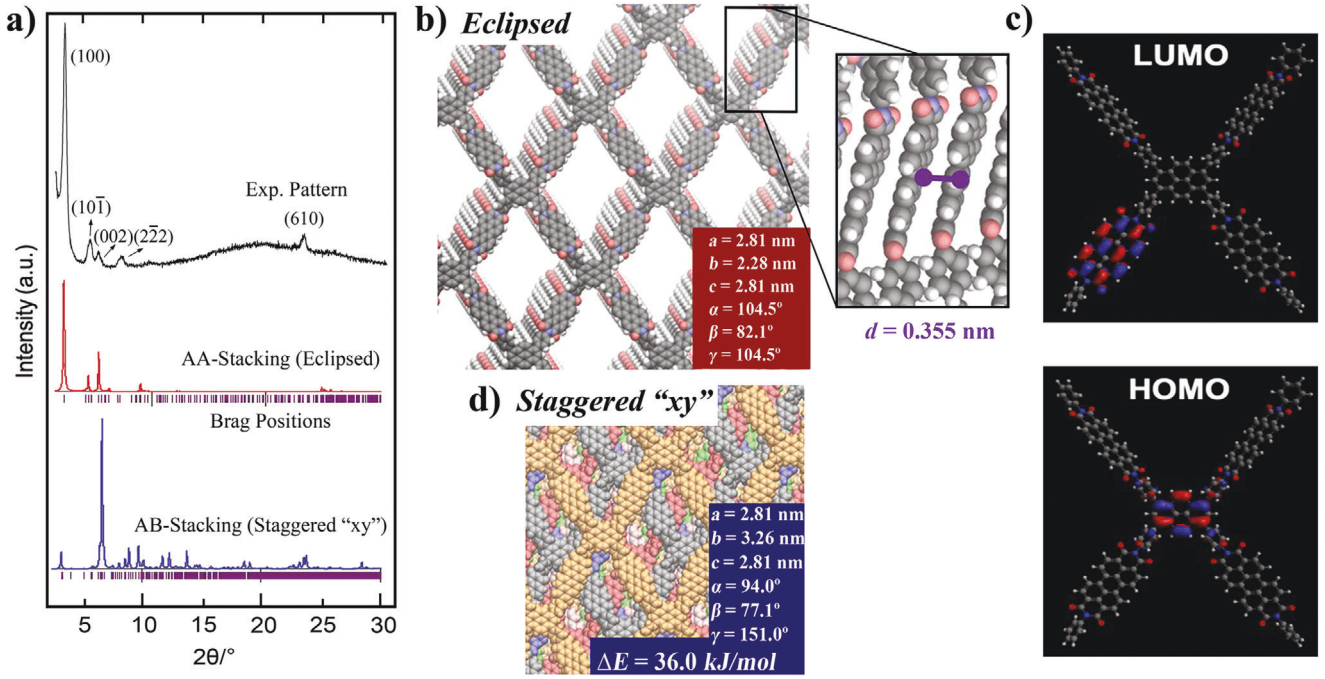


**Figure 2.** Atomistic structure of the PEPy-COF derived by utilizing quantum mechanical interatomic potentials parametrized by quantum mechanical reference data. a) Comparison of the experimentally measured (black) and simulated XRD patterns. b) Slipped eclipsed energetically preferred PEPy-COF structure. c) HOMO and LUMO orbitals of a single PEPy-COF sheet (employing a non-periodic model). d) Staggered *xy* simulated packing mode (the energy difference is given per formula unit compared to the energetically preferred slipped eclipsed structure).

interatomic potentials using solely quantum mechanical (QM) reference data (BLYP+D3/cc-pVDZ)[40–44] and used the previously introduced parametrization approach[45,46] and Tinker code.[47] By using our parametrized interatomic potentials, we systematically varied the interlayer arrangement and optimized both the geometry of the COF and the cell parameters.

Based on our calculations, we identified three different possible arrangements with high symmetry. The eclipsed arrangement was determined to be the energetically preferred packing mode of the PEPy-COF with an interlayer $\pi$–$\pi$ stacking distance of 0.355 nm (Figure 2b). Any displacement in the *x*-, *y*- or *xy*-direction led to staggered arrangements, which were higher in energy (Figure 2c,d). In both predicted staggered arrangements, staggered "*xy*" and staggered "*x*" (there was a decrease in interlayer interaction energy and thus overall higher energy was predicted; the energy change, $\Delta E$, is relative to the energetically preferred eclipsed arrangement). The higher calculated energy of the staggered "*x*" mode allowed us to eliminate this structure.

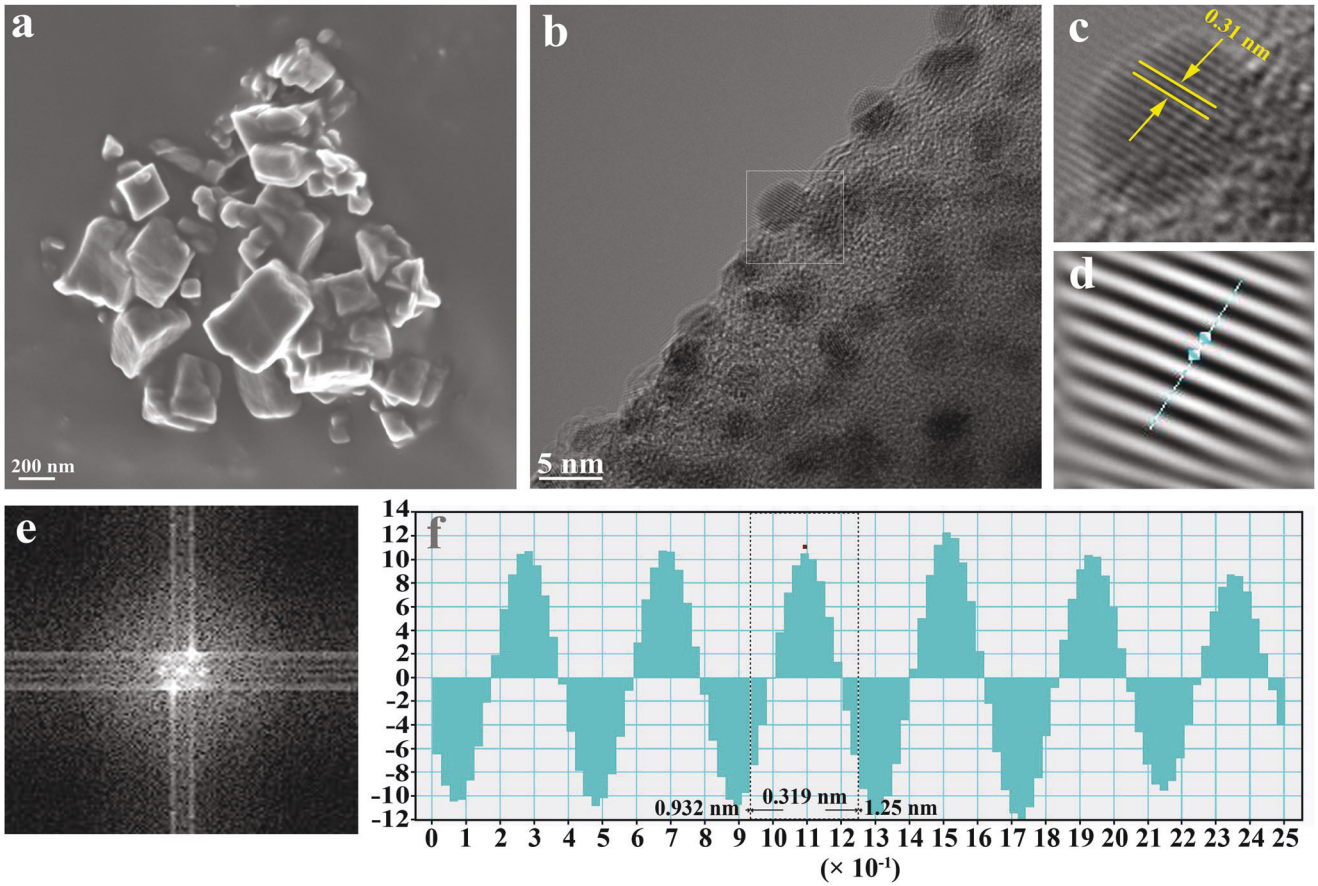


**Figure 3.** a) FE-SEM, b) HRTEM micrograph of PEPy-COF. c) Zoomed-in HRTEM image of the area marked with a white box in (b). d) Fast Fourier transformation (FFT) filter applied on (c). e) The FFT of the area marked by the white box displaying the presence of a variety of crystalline phases. f) Corresponding height profiles of the cyan line in (b).

A comparison of the simulated and experimentally measured XRD data reveals that the predicted eclipsed arrangement is in very good agreement with the experimentally observed results, providing further evidence of the eclipsed PEPy-COF structure. The highest intensity peak observed in the experimental XRD of the sample is the peak that appears at 3.75°. Good agreement was found between the experimental XRD pattern with the calculated XRD of the AA-stacking (eclipsed).[48]

A comparison of the simulated and experimentally observed XRD data revealed that the predicted eclipsed arrangement is in good agreement with the experimentally found results (Figure 2a). A small difference between the predicted and simulated data may arise because the predicted arrangements represent a perfectly crystallized COF without solvent molecules. Previous studies also reported that the solvothermal synthesis of COFs often results in small deviations from defect-free crystallinity.[49] HOMO-LUMO modeling of PEPy-COF was used to calculate the HOMO-LUMO gap was 2.62 eV (Figure 2e). The value of the band gap obtained experimentally was similar to the calculated value.

The porosity of PEPy-COF was ascertained from the $N_2$ adsorption–desorption experiment, which showed a reversible type IV isotherm with a small hysteresis curve during desorption (Figure S1, Supporting Information). The Brunauer–Emmett–Teller (BET) specific surface area for activated PEPy-COF was estimated to be 772 $m^2\ g^{-1}$ with a pore volume of 0.845 $cm^3\ g^{-1}$. The pore size distribution curve was narrow indicating that the PEPy-COF was composed of stable mesopores, and any effect of other pores or defects shaped between crystal layers was small. According to the experimental sorption data, a pore size of 3.03 nm (Figure S3, Supporting Information) was calculated. This is in line with the predicted eclipsed structure, which predicted a highly ordered open structure with large pore openings of 2.62 × 3.57 nm. Field-emission scanning electron microscopy (FE-SEM) imaging of PEPy-COF (**Figure 3**a) showed that the polymer sheets were assembled in cubic and prismatic crystal forms and the size of particles was less than 200 nm. From HRTEM, clearly aligned crystal lattice patterns were detected along the (100) plane (Figure 3b,c and Figures S4 and S5, Supporting Information). In agreement with the predicted eclipsed arrangement, the distance between the well-defined lattice fringe sheets was estimated to be 0.31 nm (predicted 0.355 nm), showing the sheet-like structure with regular orientations satisfactory for $\pi$–$\pi$ stacking (Figure 3c,d and Figure S5, Supporting Information). The fast Fourier transform (FFT) pattern showed the presence of a variety of highly crystalline phases (Figure 3e and Figure S5, Supporting Information). From the corresponding height profile in the layered area, a more accurate distance between the layers

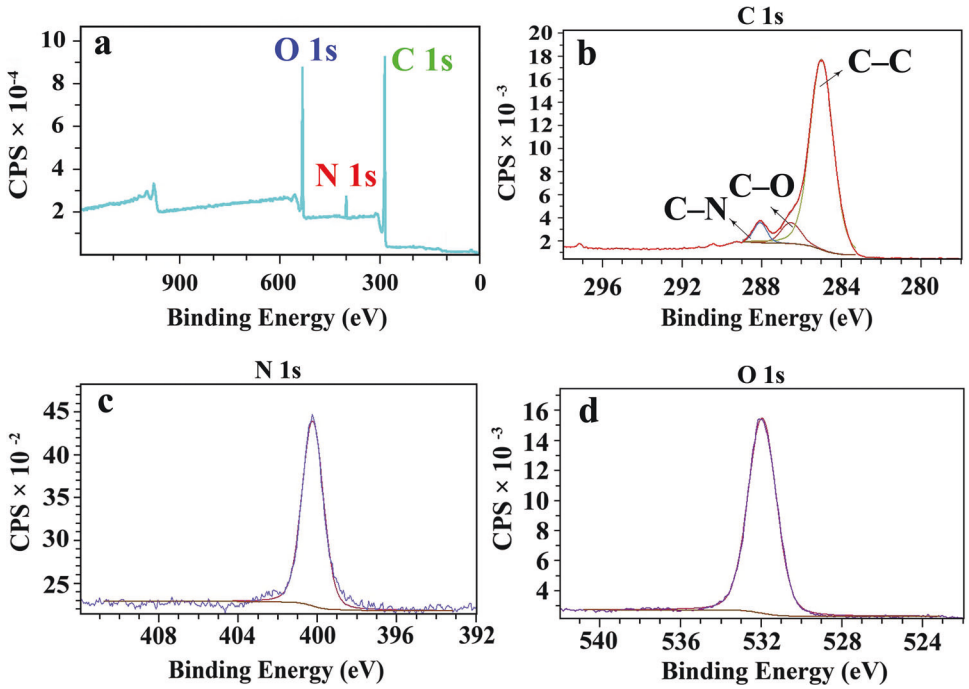


**Figure 4.** a) XPS spectrum and high-resolution XPS spectra deconvolution fit for b) C 1s, c) N 1s, and d) O 1s of PEPy-COF.

was measured (Figure 3f). Overall, the obtained FFT patterns and HRTEM images are consistent with the formation of 2D polymeric layers, where each plane contains a crystal domain.

X-ray photoelectron spectroscopic (XPS) analysis revealed the presence of C, N, and O, and an absence of impurities (**Figure 4**a). Three peaks, 284.07 eV (C–C), 286.36 (C–O), and 284.95 eV (C–N) revealed the three types of carbon atoms present after deconvolution (Figure 4b).[50] Additionally, the peak at 400.27 eV signified the presence of a nitrogen 1s level, confirming the presence of a single type of nitrogen confirmed by the deconvolution fit (Figure 4c),[51] while the peak at 532.12 eV confirmed the presence of O 1s (Figure 4d). Energy dispersive spectroscopy (EDS) elemental mapping of PEPy-COF showed the occurrence of carbon, nitrogen, and oxygen in the structure of the material (Figure S6, Supporting Information).

PEPy-COF was evaluated for thermal stability using thermogravimetric analysis (TGA). Initial weight loss occurred at 263 °C, and by 350 °C, the change in mass was ≈10% (Figure S7, Supporting Information). This was attributed to the carbon phase oxidation. At 532 °C weight loss increased, and by 800 °C, only 39.2% remained, this high char yield is attributed to the presence of the aromatic segments.

### 2.2. Photoluminescence

The solid-state UV–vis spectrum of PEPy-COF showed a broad band across the UV region, and a second broadband between 450 and 650 nm, which were attributed to photo-absorption of PTDA/PTA units and indicated that PEPy-COF could harvest photons in the visible region (Figure S8, Supporting Information).[52] From the Kubelka–Munk equation, the optical band gap ($E_g$) of PEPy-COF was calculated to be 2.62 eV, suggesting a semiconducting nature of the PEPy-COF (Figure S9, Supporting Information).

Photoluminescence microscopy showed that the particles of PEPy-COF have strong blue fluorescence (**Figure 5**a). Upon excitation in the UV region, between 310 and 410 nm, the PEPy-COF produced corresponding emission signals in the visible region. For example, under excitation at 330 nm, the PEPy-COF displayed fluorescence emission peaks at 441 and 480 nm, with a weak shoulder at 528 nm (Figure 5a and Figure S10, Supporting Information). The maximum emission peak, showed a significant non-linear and diverse red-shift as the wavelength increased indicating that, due to the large difference in energy between their lowest and highest energy levels, there was inefficient energy transfer, thus breaking Kasha's rule.[53]

PEPy-COF also exhibited high blue fluorescence when exposed to visible light (Figure S11, Supporting Information). For example, under excitation at 410 nm (Figure 5c), the PEPy-COF emitted peaks at 455, 483, and 572 nm (Figure 5a). In contrast, the starting material PTA emitted a single peak at 468 nm, while PTDA emitted two peaks at 542 and 584 nm with a shoulder at 621 nm (Figure S12, Supporting Information). The strong fluorescence of PEPy-COF upon excitation at 330 nm, represents the energy transfer from the PTA (HOMO) to the PTDA (LUMO) units along the sheet in the solid-state structure (Figure 5a and Figure S10, Supporting Information). The fluorescence decay curve is shown in Figure S13, Supporting Information, indicating that the fluorescence lifetime of PEPy-COF is 2.34 ns.

Temperature affects the fluorescence intensity of materials, and the higher the fluorescence intensity, the greater the effect of temperature.[54] A suspension of 1 mg of PEPy-COF in 15 mL of *N*,*N*′-dimethylformamide (DMF) was prepared and the fluorescence intensity, under excitation at 410 nm in the temperature range of 277–367 K was studied. The temperature working range,

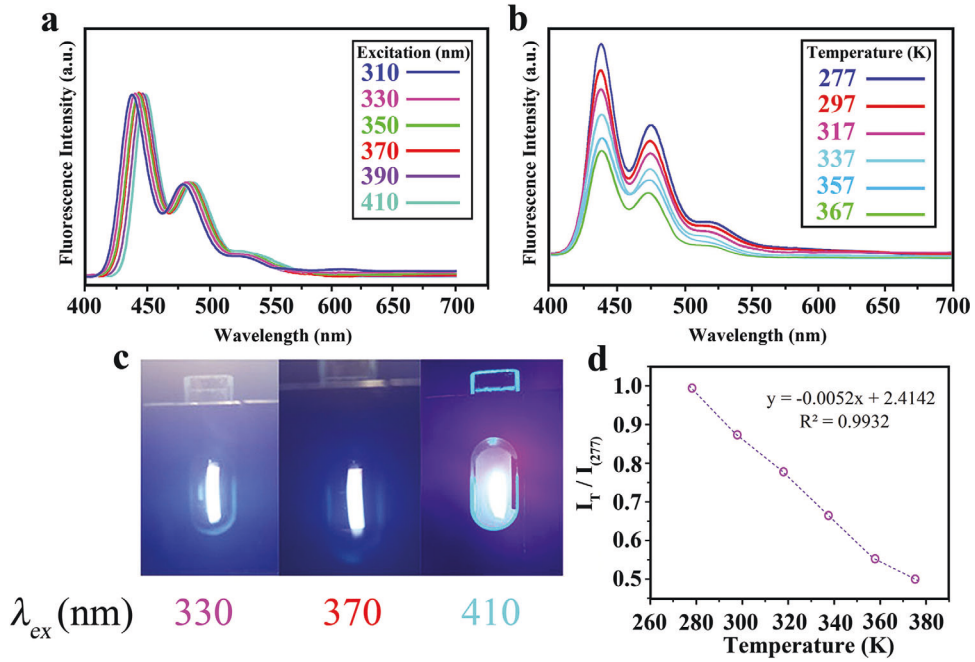


**Figure 5.** a) Fluorescence response of PEPy-COF upon excitation at a wavelength range. b) Temperature-dependent fluorescence spectra of PEPy-COF. c) Images of the PEPy-COF dispersed in DMF (1 mg in 15 mL of DMF) under excitation. d) Correlation of change of fluorescence intensity with temperature. $I_T$: Fluorescence intensity at temperature $T$, $I_{(277)}$: Fluorescence intensity at 277 K.

maximum excitation, and emission wavelength of the PEPy-COF were compared with other temperature-sensing materials such as polymers, COFs, and organic molecules (Table S1, Supporting Information). Compared to the other reported materials, PEPy-COF showed advantages such as a broad working temperature range, very good brightness, excitable in the visible range, and easy preparation without using any volatile toxic solvents.

While no change was seen in the spectral profile, some noticeable changes appeared in the emission spectra at different temperatures. The fluorescence intensity ratio (FIR), $I_T/I_{(277)}$ decreased sharply with increasing temperature (Figure 5b) and showed a linear correlation (Figure 5d). To verify that the PEPy-COF temperature-dependent fluorescent property was independent of solvent effects we dispersed the PEPy-COF in various solvents with different polarity and dielectric constants (DMF, DMSO, acetonitrile, and toluene). Due to the relative insolubility of PEPy-COF, we used ultrasound to assist in creating the dispersions. As the temperature increased from 277 to 377 K, the FIR decreased more than 50% linearly in all solvents, with only a small shift in wavelength, was observed in the maximum emission peaks (Figures S14–S21, Supporting Information). The stability of PEPy-COF in different solvent environments across a 100 K range in temperature showed that there was no solvent interference with respect to the temperature-dependent fluorescence. Compared with other anti-interference fluorescent probes based on such materials as $Eu^{3+}$-doped polymer complex,[55] metal-organic framework-polymer composite,[56] dihydrophenazine derivatives,[57] and $Er^{3+}/Yb^{3+}$-doped glass,[58] PEPy-COF showed a wider linear response region in different environments: a desirable feature in temperature-sensing devices. Most temperature-dependent fluorescent materials work in a small temperature range and they are very sensitive to high temperatures or acidic or basic media.[59] COFs with imide bonds are more stable than reported fluorescent COFs[60] and our PEPy-COF has proven to be stable over a broad range of temperatures, multiple solvents, and after treatment with ultrasound.

The possible mechanism for the decrease in the intensity with temperature, or temperature quenching of the fluorescence, is the dissociation of charge transfer excitons into free charge carriers at high temperatures. At lower temperatures, these free energy carriers undergo radiative decay because the quantity of the photon traps and structural defects are decreased due to lower molecular motion within the extended structure of the PEPy-COF.[61–68] After 370 K, no noticeable changes in the fluorescence intensity were observed. Generally, the fluorescence intensity depends on different processes, but the inherent fluorescence of a fluorophore should be independent of temperature.[61]

The decrease in fluorescence intensity and lifetime with increasing temperature is indicative of an increase in the non-radiative deactivation of the excited singlet state (Figure S22, Supporting Information). The most plausible mechanisms for high-temperature quenching in our PEPy-COF with temperature are an increase in the energy transfer between an excited electronic state and a lower electronic state without any emission of radiation (internal conversion); or energy transfer between the excited state and the solvent or solute (external conversion). In general, low temperature and high viscosity lead to increased fluorescence because they reduce the number of collisions between molecules and thus slow down the deactivation process.[69] Therefore, it is expected that as we increase the temperature of our PEPy-COF we should observe fluorescence attenuation. The ability of PEPy-COF to hold energy within its structure due to the $\pi$–$\pi$ linkages

between layers, creates the broad temperature range observed for fluorescence intensity drop.

## 3. Conclusion

We have developed a one-pot synthesis for a pyrene-based fluorescent polyimide COF with a semi-conductor band gap, and a temperature-dependent fluorescence profile. With excellent thermal stability, high surface area, and high porosity, we expect PEPy-COF to be useful for optronics applications such as components of phototransistors and photoemissive tubes. PEPy-COF like other semiconductors, can store energy in the sublayer structures and release it as light and therefore can be used in fluorescent diodes. Further, because of PEPy-COF's broad temperature range, it could be used in a temperature-sensing device based on a design similar to that reported by Wu J. L. et al.[70] The high stability and linear change of the FIR for all solvents under ultrasound conditions proves that the luminescence of PEPy-COF is robust over a wide temperature range.

## 4. Experimental Section

*Synthesis of PEPy-COF*: PTDA (10 mg, 0.025 mmol), PTA (7.22 mg, 0.12 mmol), and zinc acetate (40 mg, 0.22 mmol) were mixed in imidazole (1 g, 0.588 mmol) in a high-pressure tube. The reaction mixture was heated at 150 °C for 72 h. After cooling to room temperature, the precipitate was consecutively washed with 100 mL methanol, 50 mL of DMF, 100 mL of THF, 100 mL of acetone, and 500 mL of 10 w/v % potassium hydroxide to remove any unreacted PTDA. The filtrate was also acidified (6 M HCl) and washed with ethanol and then water (5–10 washes) to remove residual imidazole, PTA, and zinc acetate. The crude product was further purified under Soxhlet extraction with THF for 24 h. Finally, the product was dried in a vacuum oven at 70 °C for 24 h and was recovered as a vivid brick red fine powder (PEPy-COF, 19.44 mg). Yield: 85.4%. Then the sample was treated with supercritical $CO_2$ to remove any impurities from the reaction. This method was performed by pumping supercritical $CO_2$ through a fixed bed of solid substrate under a pressure of 30 MPa at 53 °C. The sample was placed in direct contact with supercritical $CO_2$ flow for 6 h. The supercritical $CO_2$ was drained away slowly and the sample was taken out of the tank. The sample was analyzed without any prior drying in the oven or in the open air. Physical Data: FT-IR (sample powder, $cm^{-1}$): 3117 (w, C–H aromatic), 1696 (m, C=O imide, asymmetric stretching), 1660 (s, C=O imide, symmetric stretching), 1611 (s), 1488 (s), 1372 (s, C–N–C axial stretching), 1228 (m, C–N–C transverse stretching), 1082 (w), 927 (m), 875 (m), 829 (m), 725 (s, C–N–C out-of-plane bending). Solid-state $^{13}C$ CP-MAS NMR (125 MHz, 25 °C, TMS) $\delta$ (ppm): 160.6, 148.92, 148.57, 145.06, 137.35, 131.39, 127.53, 124.02, 119.35, 118.88, 115.96, 114.55, 111.63, 109.88.

## Supporting Information

Supporting Information is available from the Wiley Online Library or from the author.

## Acknowledgements

The authors acknowledge The Cornell Center for Materials Research (CCMR) for the usage of their services. CCMR facilities were sponsored by the National Science Foundation under grant number DMR-1719875. This work was also supported by the National Science Foundation through the Major Research Instrument grant CHE-1531632 for Cornell University NMR Facility. The computations were done using the resources of PALMA@WWU.

## Conflict of Interest

The authors declare no conflict of interest.

## Data Availability Statement

The data that support the findings of this study are available from the corresponding author upon reasonable request.

## Keywords

covalent organic frameworks, mesoporous, optical materials, polyimide, temperature-dependent fluorescence

Received: February 17, 2023
Published online: April 27, 2023

[1] W. Zhang, L. Chen, S. Dai, C. Zhao, C. Ma, L. Wei, M. Zhu, S. Y. Chong, H. Yang, L. Liu, Y. Bai, M. Yu, Y. Xu, X.-W. Zhu, Q. Zhu, S. An, R. S. Sprick, M. A. Little, X. Wu, S. Jiang, Y. Wu, Y.-B. Zhang, H. Tian, W.-H. Zhu, A. I. Cooper, *Nature* **2022**, *604*, 72.
[2] Y. Zheng, F.-Z. Sun, X. Han, J. Xu, X.-H. Bu, *Adv. Opt. Mater.* **2020**, *8*, 2000110.
[3] S.-M. Yi, C.-R. Zhang, W. Jiang, X. Liu, C.-P. Niu, J.-X. Qi, X.-J. Chen, R.-P. Liang, J.-D. Qiu, *J. Environ. Chem. Eng.* **2022**, *10*, 107666.
[4] R. Xue, H. Guo, T. Wang, L. Gong, Y. Wang, J. Ai, D. Huang, H. Chen, W. Yang, *Anal. Methods* **2017**, *9*, 3737.
[5] S. Wan, J. Guo, J. Kim, H. Ihee, D. Jiang, *Angew. Chem., Int. Ed.* **2008**, *47*, 8826.
[6] X. Wu, X. Han, Q. Xu, Y. Liu, C. Yuan, S. Yang, Y. Liu, J. Jiang, Y. Cui, *J. Am. Chem. Soc.* **2019**, *141*, 7081.
[7] C.-R. Zhang, W.-R. Cui, W. Jiang, F.-F. Li, Y.-D. Wu, R.-P. Liang, J.-D. Qiu, *Environ. Sci.: Nano* **2020**, *7*, 842.
[8] S. Wan, J. Guo, J. Kim, H. Ihee, D. Jiang, *Angew. Chem., Int. Ed.* **2009**, *48*, 5439.
[9] C. Zhang, S. Zhang, Y. Yan, F. Xia, A. Huang, Y. Xian, *ACS Appl. Mater. Interfaces* **2017**, *9*, 13415.
[10] S.-Y. Ding, M. Dong, Y.-W. Wang, Y.-T. Chen, H.-Z. Wang, C.-Y. Su, W. Wang, *J. Am. Chem. Soc.* **2016**, *138*, 3031.
[11] A. F. M. EL-Mahdy, M.-Y. Lai, S.-W. Kuo, *J. Mater. Chem. C* **2020**, *8*, 9520.
[12] E. L. Spitler, J. W. Colson, F. J. Uribe-Romo, A. R. Woll, M. R. Giovino, A. Saldivar, W. R. Dichtel, *Angew. Chem.* **2012**, *124*, 2677.
[13] Y. Zhao, X. Wang, Y. Zhang, Y. Li, X. Yao, *J. Alloys Compd.* **2020**, *817*, 152691.
[14] P. Kumbhakar, A. K. Kole, C. S. Tiwary, S. Biswas, S. Vinod, J. Taha-Tijerina, U. Chatterjee, P. M. Ajayan, *Adv. Opt. Mater.* **2015**, *3*, 828.
[15] T. Ruf, M. Cardona, C. S. J. Pickles, R. Sussmann, *Phys. Rev. B* **2000**, *62*, 16578.
[16] E. Anjana, J. Chavda, I. Gupta, A. Kumar Mishra, *J. Photochem. Photobiol., A* **2023**, *436*, 114356.
[17] R. Flores, R. Janeiro, J. Viegas, *Sci. Rep.* **2019**, *9*, 9556.
[18] X. L. Tan, Y. F. Geng, X. J. Li, Y. L. Deng, Z. Yin, R. Gao, *IEEE Photonics J.* **2014**, *6*, 1.
[19] A. N. Starodumov, L. A. Zenteno, D. Monzon, E. De La Rosa, *Appl. Phys. Lett.* **1997**, *70*, 19.
[20] W. Yuan, Z. Yang, M. Cui, C. Yu, *IEEE Sens. J.* **2023**, *23*, 3615.
[21] W. Göpel, *Adv. Mater.* **1993**, *5*, 313.
[22] D. Havermann, J. Mathew, W. N. MacPherson, R. R. Maier, D. P. Hand, *J. Lightwave Technol.* **2014**, *33*, 2474.
[23] R. Subramanian, C. Zhu, H. Zhao, H. Li, *IEEE Photonics Technol. Lett.* **2017**, *30*, 327.

[24] A. Csaki, F. Jahn, I. Latka, T. Henkel, D. Malsch, T. Schneider, K. Schröder, K. Schuster, A. Schwuchow, R. Spittel, *Small* **2010**, *6*, 2584.
[25] N. N. Klimov, S. Mittal, M. Berger, Z. Ahmed, *Opt. Lett.* **2015**, *40*, 3934.
[26] O. S. Wolfbeis, *Adv. Mater.* **2008**, *20*, 3759.
[27] H. Peng, M. I. J. Stich, J. Yu, L. Sun, L. H. Fischer, O. S. Wolfbeis, *Adv. Mater.* **2010**, *22*, 716.
[28] M. I. J. Stich, M. Schaeferling, O. S. Wolfbeis, *Adv. Mater.* **2009**, *21*, 2216.
[29] A. Gładysiak, T. N. Nguyen, R. Bounds, A. Zacharia, G. Itskos, J. A. Reimer, K. C. Stylianou, *Chem. Sci.* **2019**, *10*, 6140.
[30] S. Dalapati, S. Jin, J. Gao, Y. Xu, A. Nagai, D. Jiang, *J. Am. Chem. Soc.* **2013**, *135*, 17310.
[31] G. Lin, H. Ding, D. Yuan, B. Wang, C. Wang, *J. Am. Chem. Soc.* **2016**, *138*, 3302.
[32] H. M. El-Kaderi, J. R. Hunt, J. L. Mendoza-Cortés, A. P. Côté, R. E. Taylor, M. O'Keeffe, O. M. Yaghi, *Science* **2007**, *316*, 268.
[33] T. Skorjanc, D. Shetty, M. Valant, *ACS Sens.* **2021**, *6*, 1461.
[34] X. Liu, Y. Han, G. Wang, Y. Wang, J. Chen, Y. Shu, J.-H. Wang, H. Qiu, *ACS Appl. Nano Mater.* **2022**, *5*, 6422.
[35] G. Chen, H.-H. Lan, S.-L. Cai, B. Sun, X.-L. Li, Z.-H. He, S.-R. Zheng, J. Fan, Y. Liu, W.-G. Zhang, *ACS Appl. Mater. Interfaces* **2019**, *11*, 12830.
[36] G. Das, B. Garai, T. Prakasam, F. Benyettou, S. Varghese, S. K. Sharma, F. Gándara, R. Pasricha, M. Baias, R. Jagannathan, N. Saleh, M. Elhabiri, M. A. Olson, A. Trabolsi, *Nat. Commun.* **2022**, *13*, 3904.
[37] K. M. Gupta, K. Zhang, J. Jiang, *Ind. Eng. Chem. Res.* **2018**, *57*, 6477.
[38] X. Yang, L. Gong, X. Liu, P. Zhang, B. Li, D. Qi, K. Wang, F. He, J. Jiang, *Angew. Chem., Int. Ed.* **2022**, *61*, e202207043.
[39] S. D. Diwakara, G. T. McCandless, S. B. Alahakoon, R. A. Smaldone, *Organic Materials* **2021**, *03*, 277.
[40] A. D. Becke, *Phys. Rev. A* **1988**, *38*, 3098.
[41] C. Lee, W. Yang, R. G. Parr, *Phys. Rev. B* **1988**, *37*, 785.
[42] Citation | Gaussian.com, https://www.gaussian.com/citation/ (accessed: November **2022**).
[43] S. Grimme, J. Antony, S. Ehrlich, H. Krieg, *J. Chem. Phys.* **2010**, *132*, 154104.
[44] A. K. Wilson, D. E. Woon, K. A. Peterson, T. H. Dunning, *J. Chem. Phys.* **1999**, *110*, 7667.
[45] S. Amirjalayer, R. Q. Snurr, R. Schmid, *J. Phys. Chem. C* **2012**, *116*, 4921.
[46] E. Kolodzeiski, S. Amirjalayer, *J. Chem. Theory Comput.* **2021**, *17*, 7010.
[47] J. W. Ponder, F. M. Richards, *J. Comput. Chem.* **1987**, *8*, 1016.
[48] P. Wang, Q. Xu, Z. Li, W. Jiang, Q. Jiang, D. Jiang, *Adv. Mater.* **2018**, *30*, 1801991.
[49] Q. Fang, Z. Zhuang, S. Gu, R. B. Kaspar, J. Zheng, J. Wang, S. Qiu, Y. Yan, *Nat. Commun.* **2014**, *5*, 4503.
[50] W. Ai, W. Zhou, Z. Du, Y. Du, H. Zhang, X. Jia, L. Xie, M. Yi, T. Yu, W. Huang, *J. Mater. Chem.* **2012**, *22*, 23439.
[51] R. J. Tseng, C. Tsai, L. Ma, J. Ouyang, C. S. Ozkan, Y. Yang, *Nat. Nanotechnol.* **2006**, *1*, 72.
[52] A. F. M. EL-Mahdy, A. M. Elewa, S.-W. Huang, H.-H. Chou, S.-W. Kuo, *Adv. Opt. Mater.* **2020**, *8*, 2000641.
[53] K. E. Henry, R. G. Balasingham, A. R. Vortherms, J. A. Platts, J. F. Valliant, M. P. Coogan, J. Zubieta, R. P. Doyle, *Chem. Sci.* **2013**, *4*, 2490.
[54] X. Wang, O. S. Wolfbeis, R. J. Meier, *Chem. Soc. Rev.* **2013**, *42*, 7834.
[55] X. Wang, R. J. Meier, M. Schäferling, S. Bange, J. M. Lupton, M. Sperber, J. Wegener, V. Ondrus, U. Beifuss, U. Henne, *Adv. Opt. Mater.* **2016**, *4*, 1854.
[56] Y. Ding, Y. Lu, K. Yu, S. Wang, D. Zhao, B. Chen, *Adv. Opt. Mater.* **2021**, *9*, 2100945.
[57] L. Shi, W. Song, C. Lian, W. Chen, J. Mei, J. Su, H. Liu, H. Tian, *Adv. Opt. Mater.* **2018**, *6*, 1800190.
[58] W. Liu, Z. Yin, D. Song, F. Zhang, B. Li, F. Wang, X. Zhang, X. Yan, T. Suzuki, Y. Ohishi, *J. Lightwave Technol.* **2022**, *40*, 7219.
[59] J. Zhou, B. del Rosal, D. Jaque, S. Uchiyama, D. Jin, *Nat. Methods* **2020**, *17*, 967.
[60] T. T. Tung, C. Pham-Huu, I. Janowska, T. Kim, M. Castro, J.-F. Feller, *Small* **2015**, *11*, 3485.
[61] N. R. Patil, R. M. Melavanki, J. Thipperudrappa, U. O. Afi, *Can. J. Phys.* **2013**, *91*, 971.
[62] B. G. Evale, S. M. Hanagodimath, M. V. Kulkarni, *J. Lumin.* **2010**, *130*, 1325.
[63] R. M. Melavanki, R. A. Kusanur, J. S. Kadadevaramath, M. V. Kulakarni, *J. Lumin.* **2009**, *129*, 1298.
[64] B. G. Evale, S. M. Hanagodimath, *Spectrochim. Acta, Part A* **2010**, *75*, 1592.
[65] S. M. Hanagodimath, B. Siddlingeshwar, J. Thipperudrappa, S. K. B. Hadimani, *J. Lumin.* **2009**, *129*, 335.
[66] V. J. P. Srivatsavoy, B. Venkataraman, N. Periasamy, *J. Photochem. Photobiol., A* **1992**, *68*, 169.
[67] T. V. Sakhno, I. V. Korotkova, O. A. Khakhel, *Theor. Exp. Chem.* **1996**, *32*, 217.
[68] A. Steinegger, I. Klimant, S. M. Borisov, *Adv. Opt. Mater.* **2017**, *5*, 1700372.
[69] M. R. Eftink, I. Gryczynski, W. Wiczk, G. Laczko, J. R. Lakowicz, *Biochemistry* **1991**, *30*, 8945.
[70] J. L. Wu, B. S. Cao, L. Rino, Y. Y. He, Z. Q. Feng, B. Dong, *RSC Adv.* **2017**, *7*, 48494.